Synthesis and optimization of furano[3,2-*d*]pyrimidines as selective spleen tyrosine kinase (Syk) inhibitors

Michael Hoemann, Noel Wilson, Maria Argiriadi, David Banach, Andrew Burchat, David Calderwood, Bruce Clapham, Phil Cox, David B. Duignan, Don Konopacki, Gagandeep Somal, Anil Vasudevan

PII: S0960-894X(16)31026-5
DOI: http://dx.doi.org/10.1016/j.bmcl.2016.09.077
Reference: BMCL 24301

To appear in: *Bioorganic & Medicinal Chemistry Letters*

Received Date: 16 August 2016
Revised Date: 28 September 2016
Accepted Date: 29 September 2016

Please cite this article as: Hoemann, M., Wilson, N., Argiriadi, M., Banach, D., Burchat, A., Calderwood, D., Clapham, B., Cox, P., Duignan, D.B., Konopacki, D., Somal, G., Vasudevan, A., Synthesis and optimization of furano[3,2-*d*]pyrimidines as selective spleen tyrosine kinase (Syk) inhibitors, *Bioorganic & Medicinal Chemistry Letters* (2016), doi: http://dx.doi.org/10.1016/j.bmcl.2016.09.077

Synthesis and optimization of furano[3,2-*d*]pyrimidines as selective spleen tyrosine kinase (Syk) inhibitors

Michael Hoemann[a],* Noel Wilson[b],* Maria Argiriadi[a], David Banach[a], Andrew Burchat[a], David Calderwood[a], Bruce Clapham[c], Phil Cox[b], David B. Duignan[a], Don Konopacki[a], Gagandeep Somal[a], Anil Vasudevan[b]

[a]*AbbVie Bioresearch Center, 100 Research Dr., Worcester MA 01545*

[b]*AbbVie, 1 North Waukegan Rd., North Chicago IL 60064*

[c]*Current Address: Reset Therapeutics, One Corporate Drive, South San Francisco CA 94080*

Abstract

A series of furano[3,2-d]pyrimidine Syk inhibitors were synthesized and optimized for their enzyme potency and selectivity versus other kinases. In addition, ADME properties were assessed and compounds were prepared with optimized profiles for *in vivo* experiments. Compound **23** was identified as having acceptable pharmacokinetic properties and demonstrated efficacy in a rat collagen induced arthritis model.

Spleen Tyrosine Kinase (Syk) is a non-receptor tyrosine kinase important for the amplification of immune signaling through Fc receptors, B-cell receptors and integrin engagement.[1] It is broadly expressed, with the highest levels in hematopoietic cells including mast cells, macrophages, neutrophils, dendritic cells, NK cells and B cells. The downstream consequences of Fc receptor signaling such as TNF release from macrophages, oxidative burst from neutrophils, IL-17 and prostanoid release from mast cells are all thought to contribute to the pathogenesis of rheumatoid arthritis (RA). Therefore, Syk inhibitors could be useful as therapeutic agents for RA as well as other immunological diseases.

Several Syk inhibitors have advanced into clinical trials. Fostamatinib is the prodrug of the active compound tamatinib (**1**), which is a non-selective kinase inhibitor and therefore not considered to be an appropriate compound to establish proof of concept for RA through inhibition of Syk.[2,3] There have been several additional Syk inhibitors reported in the clinic including Portola's PRT-062607 (**2**), Gilead's GS-9973 (**3**) and Merck's MK-8457 (**4**).[4] This paper will describe the design of a set of furano[3,2-*d*]pyrimidines that are selective inhibitors of

Syk, along with how we optimized their profile to support their progression into *in vivo* models of arthritis.

Figure 1. Known Syk inhibitors and starting furano[3,2-*d*]pyrimdine **6**

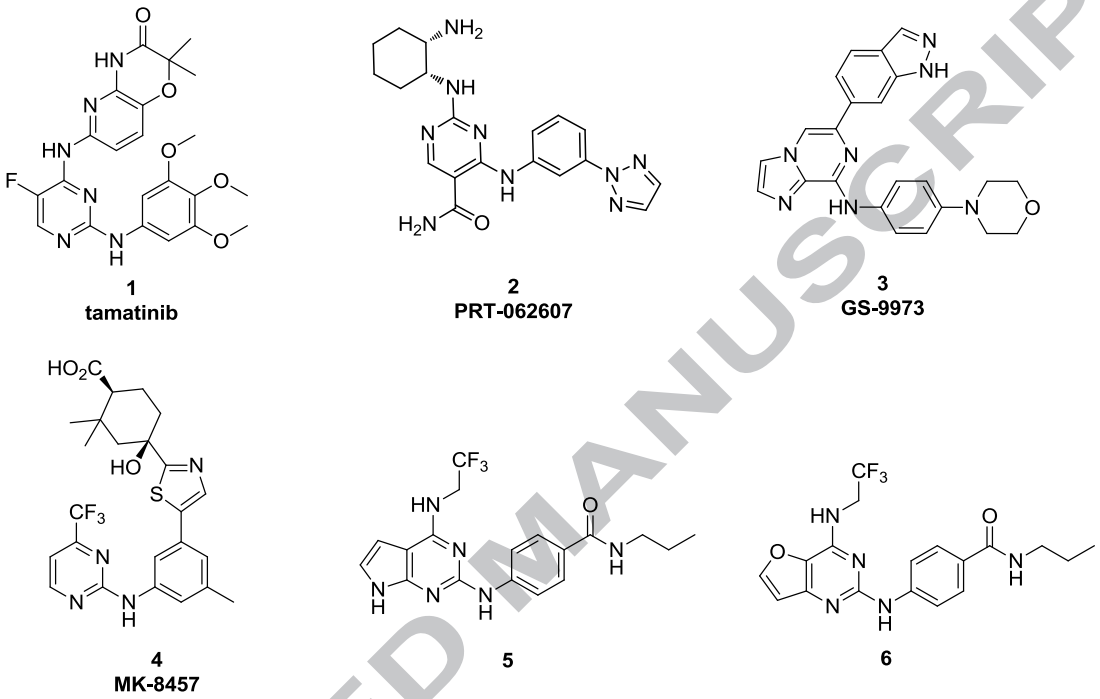

Our entry into the furano[3,2-*d*]pyrimidine series started from the thoroughly explored pyrrolo[2,3-*d*]pyrimidine scaffold from which inhibitors for many kinases such as Jak's [5a], Src[5b], Akt[5c], BTK[5d] and PDK1[5e] have been described. More recently, GSK disclosed on a series of pyrrolo[2,3-*d*]pyrimidine Syk inhibitors with compound **5** being a representative example.[6] It is widely recognized that pyrrolo[2,3-*d*]pyrimidine kinase inhibitors suffer from poor kinase selectivity due predominantly to the H-bond donor-acceptor-donor motif comprising the hinge-binding element. We reasoned that replacing one of the hinge H-bond donors with a C-H would attenuate the hinge-binding potential, and through optimization of interactions with more distal residues afford a more selective inhibitor. To test this hypothesis, the furano[3,2-*d*]pyrimidine compound **6** was synthesized and showed a ~30-fold reduction in Syk potency (Table 1). The potency of this first analog was too weak to establish an improved selectivity profile and the

strategy focused on targeting other regions of the protein binding site to enhance binding potency.

Table 1. Syk enzyme potency

Compound	Syk IC_{50} (μM)[a]
5	0.017
6	0.561

[a] Syk IC_{50} determined using an HTRF format (see supplementary material for details)

Our optimization strategy was based on a structural model of **6** in Syk to identify potential interactions that could improve the Syk affinity. We constructed the model from the tamatinib crystal structure (PDB code 3FQS)[7] using Glide software[8]. The model (Figure 2) showed two distinct hinge interactions of the furano[3,2-*d*]pyrimidine core with the Ala451 NH and C=O. The propylbenzamide was directed towards the extended hinge region while the trifluoroethylamine was positioned under the glycine rich loop. One key structural feature in the Syk ATP binding pocket is the relatively rare Pro455 residue with only 8 other kinases having a proline at this position. In Syk, Pro455 creates a narrow channel at the extended hinge region and presents an opportunity to make favorable CH/π interactions with aromatic ring systems.[9]

Figure 2. Model of Compound **6** in the catalytic domain of human Syk Kinase. This model was based on crystal structure of Tamatinib bound to Syk (PDB code: 3FQS)

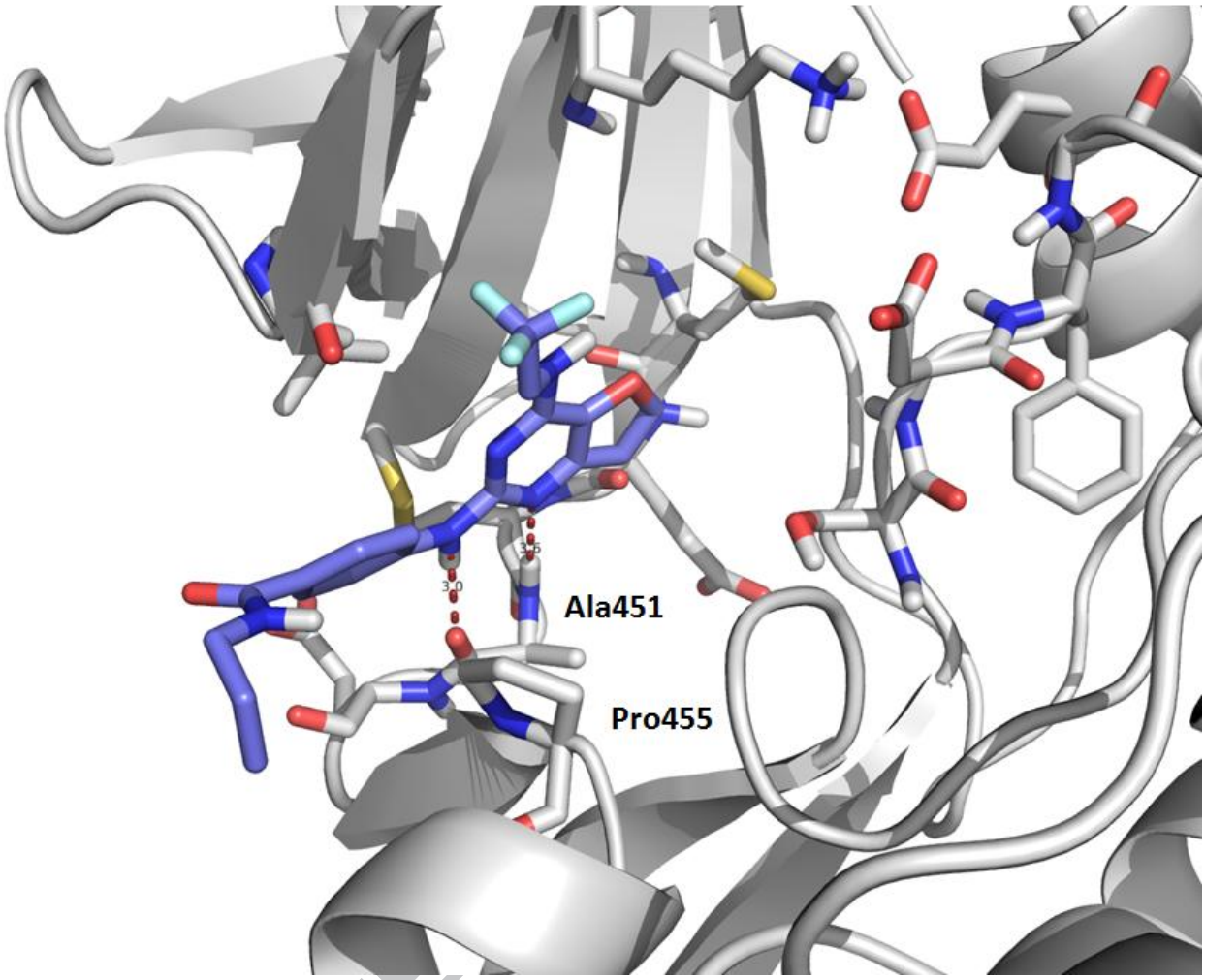

The general synthesis of disubstituted furano[3,2-*d*]pyrimidine analogs began with commercially available 2,4-dichlorofurano[3,2-*d*]pyrimidine **24** as illustrated in Scheme 1. Nucleophilic aromatic substitution (S_NAr) of **24** with various amines and subsequent Buchwald coupling or S_NAr allowed rapid access to analogues **6-20**, **23**, and **26**.[10] Primary amines used in the Buchwald reaction were commercially available or were obtained via reduction of the corresponding commercial nitro compound using standard literature methods (Scheme 1, step iv), or by the syntheses outlined in Schemes 3 and 4. The homochiral products **21** and **22** were isolated using chiral HPLC of racemic intermediates **26** (Scheme 2).[11]

Scheme 1.

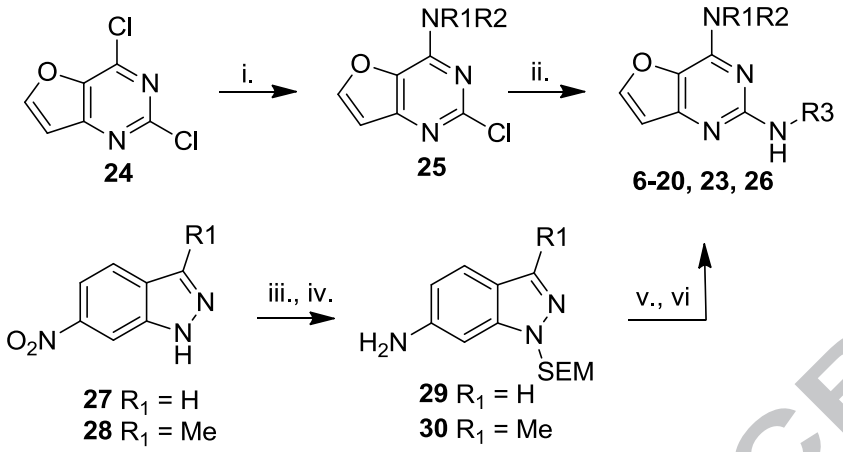

Reagents and conditions: (i) NHR1R2, TEA, 1,4-dioxane, 83-99% (ii) NH_2R3, Pd_2dba_3, X-Phos, K_2CO_3 or KOt-Bu, t-BuOH or 1,4-dioxane, 85 -110 ºC, 8-48% or (-)-camphor-10-sulfonic acid, iPrOH, 90 ºC, 54-70% (iii) NaH, THF, 0 ºC, 30 min then SEM-Cl, 0 ºC – rt, 59-90% (iv) H_2, Pd/C, MeOH (v) **25**, Pd_2dba_3, X-Phos, K_2CO_3, 1,4-dioxane, 110 ºC, 75-100% or **25**, Pd_2dba_3, X-Phos, KOt-Bu, 1,4-dioxane, 100 ºC, μW, 65% (vi) TFA, DCM, 30 ºC, 19-60%

Scheme 2.

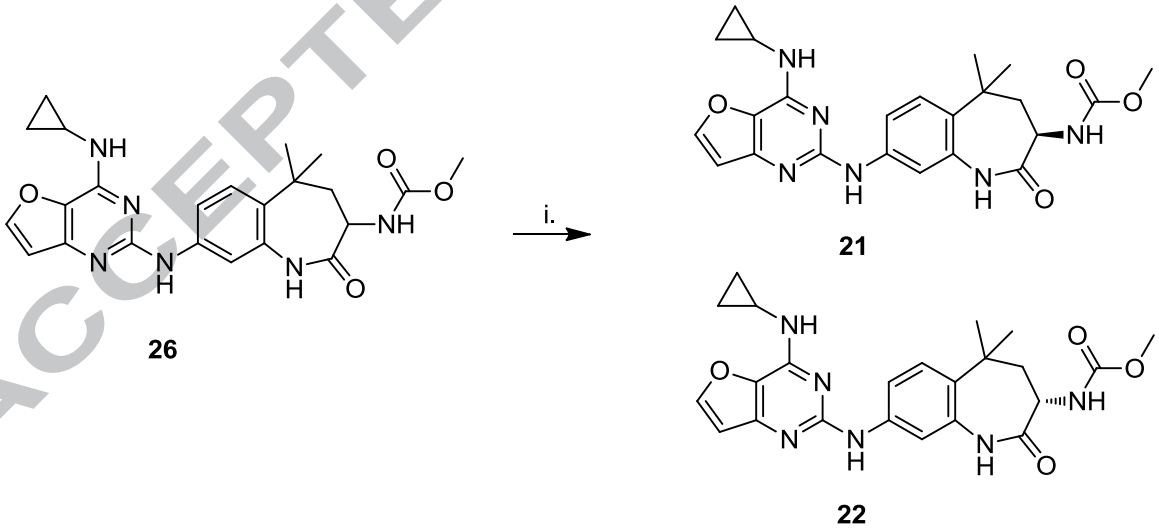

Reagents and conditions: (i) Chiral HPLC purification

Targets bearing an indazole in the extended hinge region required a protecting group strategy as the unprotected indazole yielded two regioisomers as products. While Boc protection was adequate, the best strategy was protection of commercially available indazoles, **27** and **28**, with a SEM group. Reduction of the nitro group afforded the protected aminoindazoles **29** and **30**. Palladium-catalyzed amination of **25** with the protected indazoles followed by removal of the protecting group afforded furano[3,2-*d*]pyrimidines **8**, **9**, and **19**.

Scheme 3.

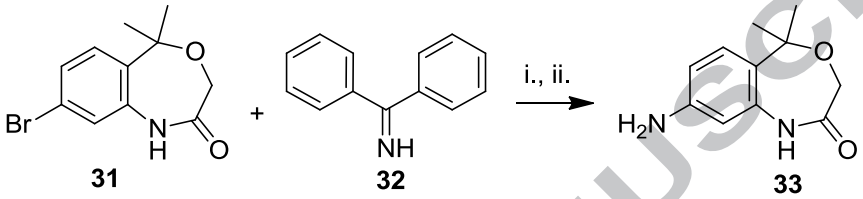

Reagents and conditions: (i) $Pd(OAc)_2$, Xantphos, Cs_2CO_3, TEA, 1,4-dioxane, 90 ºC, 77-91% (ii) 1M HCl, THF, 0 ºC, 70-87%

Scheme 4.

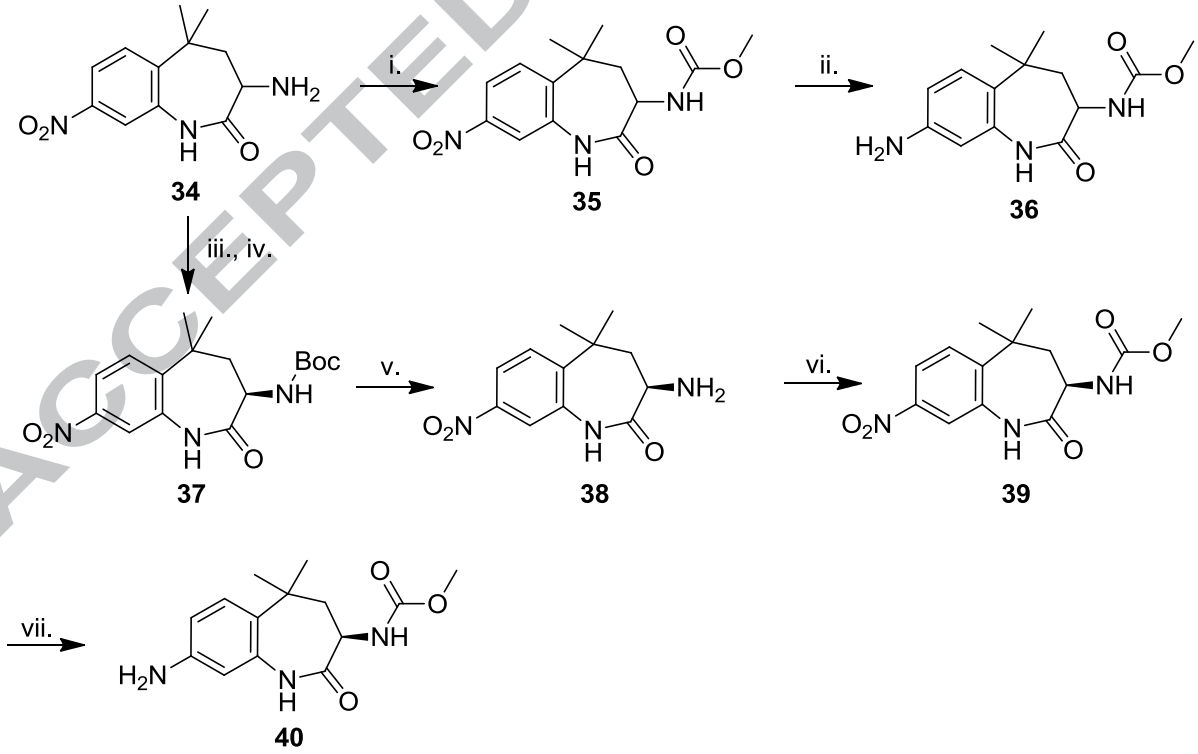

Reagents and conditions: (i) Methylchloroformate, DIEA, DCM, 5 ºC, 81-97% (ii) H_2, 10% Pd/C, 1:1 EtOAc/MeOH, 72-100% (iii) Boc_2O, $NaHCO_3$, 5:1 DCM/water (iv) Chiral HPLC purification, 40% over 2 steps (v) 4M HCl in 1,4-dioxane (vi) Methylchloroformate, DIEA, DCM, 5 ºC, 100% (vii) H_2, 10% Pd/C, 1.7:1 EtOAc/MeOH, 81-95%

Azepinones **33**, **36** and **40** were synthesized according to Schemes 3 and 4. Amination of benzoxazepinone **31**[12] using benzophenone imine as an ammonia surrogate provided amine intermediate **33**. Treatment of azepinone **34**[13] with methyl chloroformate provided carbamate **35**. Reduction of the nitro group using Pd/C gave the racemic azepinone **36**. Homochiral intermediate **37** was obtained after protecting azepinone **34** and chiral HPLC separation. The separated *tert*-butyl carbamate **37** was exchanged for the methyl carbamate to provide **39** using standard deprotection/protection methods. Reduction of the nitro group with H_2/Pd afforded aniline **40**.

The loss in Syk affinity as a result of the core switch could be regained through modification to the extended hinge group as shown in Table 2. While maintaining the trifluoroethylamino group at the 4-position, modification of the phenyl group to **7** or the fusion of an additional ring as in **8,** yielded about an 8-fold improvement in potency from **6**. In addition, adding modest steric bulk in the form of a methyl group to the 3-position of the indazole provided a further modest boost in potency as shown with compound **9**. In order to mitigate the presence of four aromatic rings in compounds **8** and **9**, we prepared bicyclic analogs with a saturated ring giving **10**, **11**, and **12**. These bicycles were well tolerated and led to compounds with improved lipophilic ligand efficiency (LLE), such as **13** (LLE = 5.10).[14] In addition, as Syk enzyme potency was enhanced, it correlated well with enhanced cellular potency (Table 2).

Table 2. SAR for initial analogs

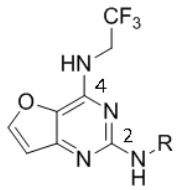

Cmpd	R	Syk IC_{50} (μM)[a]	Ramos B-Cell EC_{50} (μM)[b]	Rat Cl,mic unbound (L/hr/kg)	LLE
6	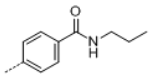	0.561	0.346	No Data	1.73
7	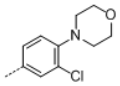	0.061	0.117	96.0	2.25
8		0.081	0.235	15.3	2.82
9		0.047	0.087	No Data	2.79
10	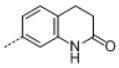	0.063	0.101	21.9	3.34
11	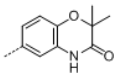	0.179	0.723	10.6	3.05
12	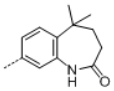	0.043	0.049	52.8	2.07
13	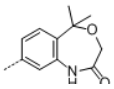	0.007	0.017	<4.9	5.10

[a] Syk IC_{50} determined using an HTRF format (see supplementary material for details)

[b] Ramos B-cell IC_{50} determined using an Ca^{+2} flux format (see supplementary material for details)

[c] LLE is derived from the pIC50 – cLog P (Biobyte)[14]

With the improved Syk affinity, we next assessed the kinome selectivity of several analogs utilizing an internal panel of 75 kinases in a TR-FRET format (Figure 3). We evaluated the kinome profile of the pyrrolopyrimidine **5** as well as several furanopyrimidines from Table 2. We were encouraged to see that the furanopyrimidines displayed a much improved selectivity profile over the pyrrolopyrimidine **5**. Compound **5** has nine kinases within 10x of the enzyme IC_{50} while **7** has a single kinase within 10x and **8** and **13** have none. In fact **13** has only two kinases (Src and Fyn) at less than 30x, validating the hypothesis that removing one of the H-bond donors from the hinge would result in an improved kinome profile.

Figure 3. Kinome profiling for furano[3,2-*d*]pyrimdine Syk inhibitors.

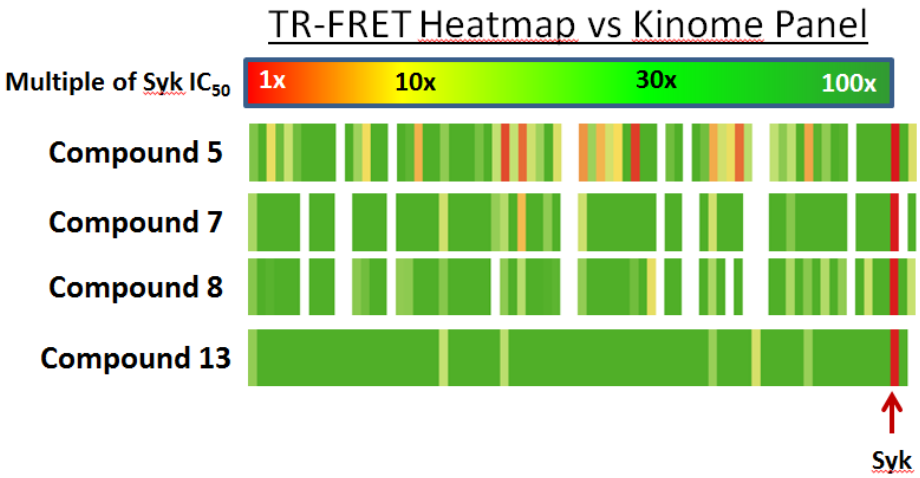

A white bar within the heatmap denotes no data for that particular kinase as the panel changed over the course of the project (See supplemental section for data)

While **13** showed very good enzyme and cellular potency, and had acceptable properties in terms of unbound clearance in rat microsome incubation, it suffered from poor solubility (4.96 μM, Fed SSIF pH 5).[15] In addition, the trifluoroethyl group contributed a significant amount of molecular weight and calculated lipophilicity. Therefore, we set out to scan the 4-position to find a suitable replacement (Table 3). The ethyl analog, **14**, provided a significant improvement in solubility, yet suffered from increased rat microsomal clearance. This trend continued with extended alkyl chains **15** as well as branched alkyl chains **16**, which also exhibited a loss in potency. Incorporation of a cyclopropyl group in **18** provided the optimal balanced set of attributes related to potency, clearance and solubility

Table 3. SAR and optimization for solubility and clearance

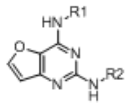

Cmpd	R1	R2	Syk IC_{50} (μM)[a]	Ramos B-Cell EC_{50} (μM)[b]	Rat Cl,mic unbound (L/hr/kg)	Human Cl,mic unbound (L/hr/Kg)	Solubility Fed SSIF pH5 (μM)	LLE
13	$-CH_2CF_3$		0.007	0.017	<4.9	10.2	4.96	5.10
14	$-CH_2CH_3$		0.006	0.018	19.1	5.5	>67	5.43
15	$-CH_2CH_2CH_3$		0.045	0.030	22.4	18.4	>200	4.03
16	$-CH_2CH_2(CH_3)_2$		0.064	0.043	64.5	30.4		3.47
17	$-CH_2(CH_3)_2$		0.013	0.030				4.79
18	-c-Pr		0.005	0.018	12.0	7.2	158	5.45
19	-c-Pr		0.023	0.034			99	3.31
20	-c-Pr		0.005	0.035	23.8	19.0		3.21
21	-c-Pr	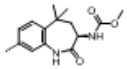	0.012	0.039	10.9	7.4	27	4.31
22	-c-Pr	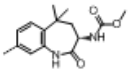	1.37		19.9	7.1		2.25
23	$-CH_2CHF_2$	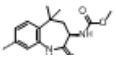	0.020	0.026	10.6	<2.3	>67	4.10

We obtained a crystal structure of Compound **19** bound to the catalytic domain (amino acids 363-639) of human Syk (Structure methods, data and structure refinement are described in the Supplemental Methods; PDB Code 5T68). Compound **19** is a potent Syk inhibitor (Enzyme IC_{50} = 0.023 μM; Ramos B-Cell EC_{50} = 0.033 μM). The structure confirmed the donor-acceptor hinge binding interactions of the furanopyrimidine core with distances of 2.8 Å to the acceptor NH of Ala451 and 2.6 Å to the donor carbonyl group of Ala451. The structure also confirmed the interaction of the indazole ring with Pro455 measured at a distance of 4.0 Å (**Figure 4**). Proline-aromatic interactions are routinely observed in protein structures and also reported in Isostar.[16] An additional interaction was observed between the NH of the indazole and the carbonyl group of glycine rich loop residue Leu377. We found that the combination of a 1) donor-acceptor hinge interaction with 2) stabilization of the glycine rich loop via Leu377 and 3)

long range aromatic interaction with Pro455 led to an excellent selectivity profile in our internal TR-FRET kinase panel (64 kinases with IC_{50}'s > 1.0 μM). The cyclopropyl moiety did not appear to be making any direct interactions with the protein and most likely contributed to filling void space in the ATP binding pocket. *In silico* water analysis using the Shrödinger Maestro WaterMap software generated water with calculated energies in the apo form of Syk. Destabilized waters (ΔG 2 to 3 kcal/mol) were identified in the cyclopropyl binding pocket suggesting that this area could be displaced by hydrophobic groups.[17]

Figure 4. X-ray crystal structure of Compound **19**

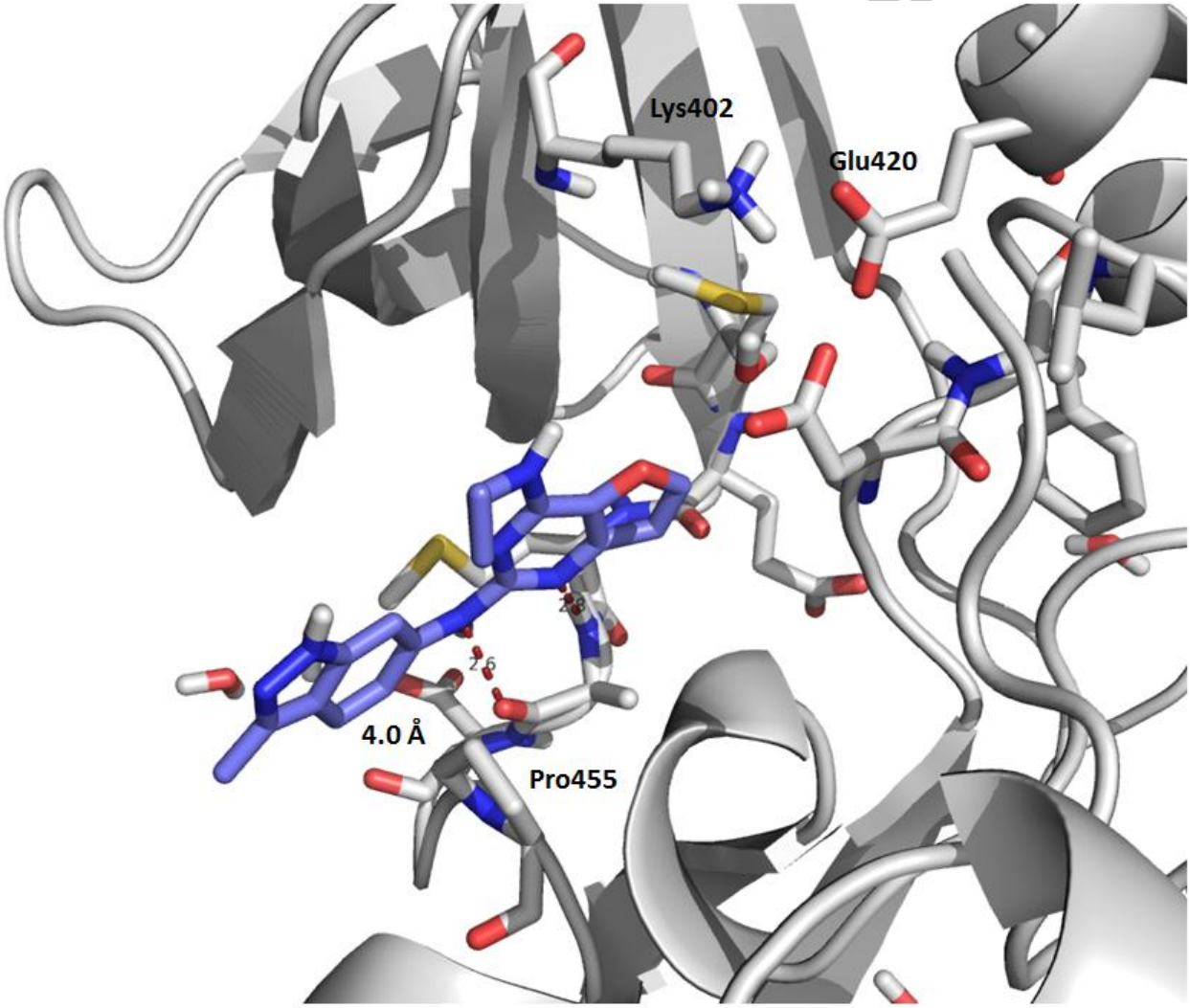

As with any medicinal chemistry program, there was a need to optimize ADME properties for this series based on data from our initial screens. In particular, for **18** and **19**, it was found that these compounds displayed significant time-dependent inhibition (TDI) of CYP3A4 in human

liver microsomes (Table 4). In general, the TDI was observed when the 4-position contained a cyclopropylamino group. For example, **13** had a lower decrease in enzyme activity. This observation is supported by literature reports of compounds containing cyclopropylamines moieties that exhibit TDI of CYP3A4.[18] Therefore, even though **19** exhibited low microsomal clearance, the TDI liability led us to use other substituents at this position.

Table 4. *In vitro* time-dependent inhibition of CYP3A4 in human liver microsomes

Compound	Concentration (μM)	% Activity at 0 minutes	% Activity Remaining at 30 minutes
13	10	91	81
	50	92	75
18	10	97	56
	50	80	14
19	10	94	51
	50	87	28

In addition, based on the high cLog P values and early *in vivo* PK data (data not shown), we continued to look for ways to minimize the *in vivo* clearance of these compounds. This series had a good *in vitro* / *in vivo* correlation between unbound rat microsomal clearance and unbound plasma clearance from rat pharmacokinetic (PK) experiments. This enabled the use of *in vitro* microsomal clearance data to select compounds to move forward into *in vivo* experiments. The data suggested that the addition of an exocyclic methyl carbamate (**20** to **21**) could reduce mouse and human clearance, probably due to the relative decrease in cLog P (5.09 to 3.61). For the exocyclic carbamates, one enantiomer was more potent than the other (Compare **21** with **22**) and this was a consistent finding (~10 to 100x) irrespective of the carbamate group or the 4-substituent. Compound **23** did not exhibit CYP3A4 TDI and had a low rate of *in vitro* microsomoal clearance in both mouse and human. Due to its acceptable PK profile in both rat and dog (Table 5), **23** was selected for further *in vivo* experiments. We chose to evaluate the role of **23** in rat collagen induced arthritis (CIA) because this model shares many similarities with human rheumatoid arthritis. In particular, the development of arthritis relies upon breach of tolerance and generation of antibodies to collagen and self, which are modulated by Syk dependent cellular processes. Compound **23** was dosed orally in the rat CIA model at 0.3,1, 3, 0 and 30 mg/kg b.i.d. Treatment began at first signs of clinical disease and continued for 8 days until the end of the experiment. Administration of **23** resulted in a dose dependent decrease in paw swelling achieving 75% inhibition at 10 mg/kg and 95% inhibition at 30 mg/kg, the same

degree of efficacy as seen with prednisolone treatment. The compound was well tolerated throughout the study. The ED_{50} was 9 mg/kg corresponding to a day last AUC_{50} (0-12 h) of 3.9 μg*hr/mL. Compound **23** did not show any liabilities in an *in vitro* safety panel (Ames >100 mM , hERG IC_{50} >20 μM, and HepG2 cytotoxicity IC_{20} >10 μM).

Table 5. Rat and Dog Pharmaokinetcs for **23**

Species	Dose (mg.kg)	i.v.			p.o.		
		Cl (L/hr/kg)	$T_{1/2}$ (h)	V_{ss} (L/kg)	F (%)	AUC (μg*hr/mL)	C_{max} (ng/mL)
Rat	1	1.7	2.0	4.6	27	0.18	36
Dog	1	0.17	9.9	2.3	40	2.34	151

Figure 5. Rat CIA data for Compound **23**

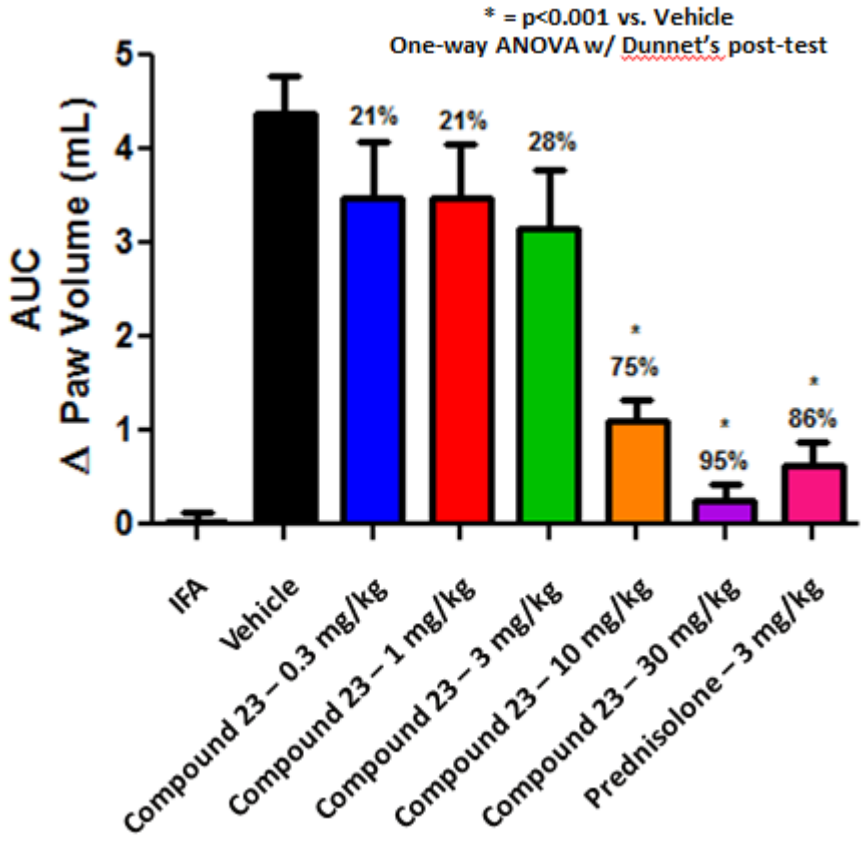

In summary, we report the discovery of furano[3,2-*d*]pyrimidines as novel and selective Syk inhibitors. The initial lead **6** was optimized for potency as well as kinase selectivity by targeting interactions with Pro455 in the kinase pocket. Liabilities including time–dependent CYP3A4 inhibition as well as high microsomal clearance were observed. Optimization to address these multiple liabilities led to **23** which possessed good PK in both rat and dog and demonstrated efficacy in a rat CIA model.

References and notes

Use of the IMCA-CAT beamline 17-ID (or 17-BM) at the Advanced Photon Source was supported by the companies of the Industrial Macromolecular Crystallography Association through a contract with Hauptman-Woodward Medical Research Institute.

Use of the Advanced Photon Source was supported by the U.S. Department of Energy, Office of Science, Office of Basic Energy Sciences, under Contract No. DE-AC02-06CH11357.

Disclosures

Michael Hoemann, Noel Wilson, Maria Argiriadi, David Banach, Andrew Burchat, David Calderwood, Phil Cox, David Duignan, Don Konopacki, Gagandeep Somal and Anil Vasudevan are employees of Abbvie. Bruce Clapham was an employee of AbbVie at the time of the work. The design, study conduct and financial support for this research were provided by AbbVie. AbbVie participated in the interpretation of data, review and approval of the publication.

References and notes

1. (a) Kaur, M.; Singh, M.; Silakari, O. *Eur. J. Med. Chem.* **2013**, *67*, 434. (b) Tan, S.-L.; Lioa, C.; Lucas, M. C.; Stevenson, C.; DeMartino, J. A. *Pharmacol. Ther.* **2013**, *138*, 294.
2. Weinblatt, M. E.; Kavanaugh, A.; Genovese, M. C.; Jones, D. A.; Musser, T. K.; Grossbard, E. B.; Magilavy, D. B. *J. Rheumatol.*, **2013**, *40*, 369.
3. (a) Braselmann, S.; Taylor, V.; Zhao, H.; Wang, S.; Sylvain, C.; Baluom, M.; Qu, K.; Herlaar, E.; Lau, A.; Young, C.; Wong, B. R.; Lovell, S.; Sun, T.; Park, G.; Argade, A.; Jurcevic, S.; Pine, P.; Singh, R.; Grossbard, E. B.; Payan, D. G.; Masuda, E. S. *J. Pharm. Exp. Ther.* **2006**, *319*, 998. (b) Ellis, J. M.; Altman, M. D.; Bass, A.; Butcher, J. W.;

Byford, A. J.; Donofrio, A.; Galloway, S.; Haidle, A. M.; Jewell, J; Kelly, N.; Leccese, E. K.; Lee, S.; Maddess, M.; Miller, J. R.; Moy, L. Y.; Osimboni, E.; Otte, R. D.; Reddy, M. V.; Spencer, K.; Sun, B.; Vincent, S. H.; Ward, G. J.; Woo, G. H. C.; Yang, C.; Houshyar, H.; Northrup, A. B. *J. Med. Chem.* **2015**, *58*, 1929.

4. (a) Coffey, G.; DeGuzman, F.; Inagaki, M.; Pak, Y.; Delaney, S. M.; Ives, D.; Betz, A.; Jia, Z. J.; Pandey, A.; Baker, D.; Hollenbach, S. J.; Phillips, D. R.; Sinha, U. *J. Pharm. Exp. Ther.* **2012**, *340*, 350; (b) Currie, K. S.; Kropf, J. E.; Lee, T.; Blomgren, P.; Xu, J.; Zhao, Z.; Gallion, S.; Whitney, J. A.; Maclin, D.; Lansdon, E. B.; Maceijewski, P.; Rossi, A. M.; Rong, H.; Macaluso, J.; Barbosa, J.; Di Paolo, J. A. and Mitchell, S. A. *J. Med. Chem.* **2014**, *57*, 3856.
5. (a) Jiang, J.-K.; Ghoreschi, K.; Deflorian, F.; Chen, Z.; Perreira, M.; Pesu M.; Smith, J.; Nguyen, D.-T.; Liu, E. H.; Leister, W.; Costanzi, S.; O'Shea, J. J.; Thomas, C. J. *J. Med. Chem.* **2008**, *51*, 8012; (b) Dincer, S.; Cetin, K. T.; Onay-Besikci, A.; Olgen, Sureyya *J. of Enzyme Inhib.* **2013**, *28*, 1080; (c) Addie, M. Ballard, P.; Buttar, D.; Crafter, C.; Currie, G.; Davies, B. R.; Debreczeni, J.; Dry, H.; Dudley, P.; Greenwood, R.; Johnson, P. D.; Kettle, J. G.; Lane, C.; Lamont, G.; Leach, A.; Luke, R. W. A.; Morris, J.; Ogilvie, D.; Page, K.; Pass, M.; Pearson, S.; Ruston L. *J. Med. Chem.* **2013**, *56*, 2059; (d) Zhao, X.; Huang, W.; Wang, Y.; Xin, M.; Jin, Q.; Cai, J.; Tang, F.; Zhao, Y.; Xiang, H. *Bioorg. Med. Chem.* **2015**, *23*, 891; (e) O'Brien, N. J.; Brzozowski, M.; Buskes, M. J.; Deady, L. W.; Abbott, B. M. *Bioorg. Med. Chem.* **2014**, *22*, 3879.
6. Gore, P. M.; Patel, V. K.; Walker, A. L.; Woodrow, M WO 2007/042298 A1, **2007**.
7. Villasenor, A. G.; Kondru, R.; Ho, H.; Wang, S.; Papp, E.; Shaw, D.; Barnett, J. W.; Browner, M. F.; Kuglstatter, A. *Chem. Biol. Drug Des.* **2009**, *73*, 466.
8. Halgren, T. A.; Murphy, R. B.; Friesner, R. A.; Beard, H. S.; Frye, L. L.; Pollard, W. T.; Banks, J. L. *J. Med. Chem.* **2004**, *47*, 1750.
9. (a) Zondlo, N. J. *Acc. Chem. Res.* **2013**, *46*, 1039. (b) Leitgeb, B.; Toth, G. *Eur. J. Med. Chem.* **2005**, *40*, 674.
10. Methods and experimentals for the preparation of the compounds can be found in WO 2012/048222, **2012** and the supplementary materials.

11. Weinberg, L. R.; Albom, M. S.; Angeles, T. S. ; Husten, J.; Lisko, J. G.; McHugh, R. J.; Milkiewicz, K. L.; Murthy, S.; Ott, G. R.; Theroff, J. P.; Tripathy, R.; Underiner, T. L.; Zificsak, C. A.; Dorsey, B. D. *Bioorg. Med. Chem. Lett.* **2011**, *21*, 164
12. Zhang, P.; Kern, J. C.; Terefenko, E. A.; Fensome, A.; Unwalla, R.; Zhang, Z.; Cohen, J.; Berrodin, T. J.; Yudt, M. R.; Winneker, R. C.; Wrobel, J. *Bioorg. Med. Chem.* **2008**, *16*, 6589
13. Milkiewicz, K. L.; Aimone, L. D.; Albom, M. S; Angeles, T. S.; Chang, H.; Grobelny, J. V.; Husten, J.; LoSardo, C.; Miknyoczki, S.; Murthy, S.; Rolon-Steele, D.; Underiner, T. L.; Weinberg, L. R.; Worrell, C. S.; Zeigler, K. S.; Dorsey, B. D. *Bioorg. Med. Chem.* **2011**, *19*, 6274.
14. Hopkins, A. L.; Keseru, G. M.; Leeson, P.; Rees, D. C.; Reynolds, C. H. *Nat. Rev. Drug Disc.* **2014**, *13*, 105.
15. The Fed SSIF solubility assay is a thermodynamic determination using dry powder that is equilibrated with a buffer (pH 5) for 2 days. The resulting mixture is filtered and the filtrate is analyzed by HPLC versus a standard concentration curve. See Supplementary Material for details.
16. Isostar: A library of information about non-bonded interactions; Bruno, I.J.; Cole, J. C.; Lommerse, J. P. M.; Rowland, R. S.; Taylor, R.; Verdonnk, M. L. *J. Comput. Aided Mol. Des.* **1997**, *11*, 525.
17. Schrödinger Release 2015-3: WaterMap, version 2.4, Schrödinger, LLC, New York, NY, 2015; (a) Abel, R.; Young, T.; Farid, R.; Berne, B. J.; Freisner, R. A. *J. Am. Chem. Soc.* **2008**, *130*, 2817; (b) Young, T.; Abel, R.; Kim, B.; Berne, B. J.; Freisner, R. A. *Proc. Natl. Acad. Sci. U.S.A.* **2007**, *104*, 808.
18. (a) Orr, S. T. M.; Ripp, S. L.; Ballard. T. E.; Henderson, J. L.; Scott, D. O.; Obach, R. S.; Sun, H.; Kalgutkar A. S. *J. Med. Chem.* **2013**, *55*, 4896; (b) Chen, A.; Dubé, D.; Dubé, L.;Gagné, S.; Gallant, M.; Gaudreault, M.; Grimm, E.; Houle, R.; Lacombe, P.; Laliberté, S.; Liu, S.; MacDonald, D.; Mackay, B.; Martin, D; McKay, D.; Powell, D.; Lévesque, J.-F. *Bioorg. Med. Chem. Lett.* **2010**, *20* 5074.

Graphical abstract

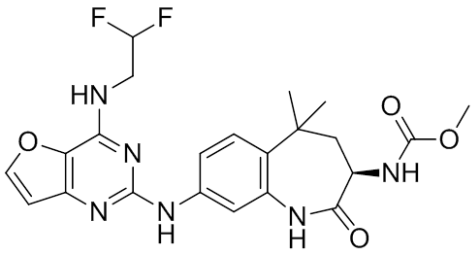

Compound 23

Syk IC_{50} = 20 nM
Ramos B-Cell EC_{50} = 26 nM

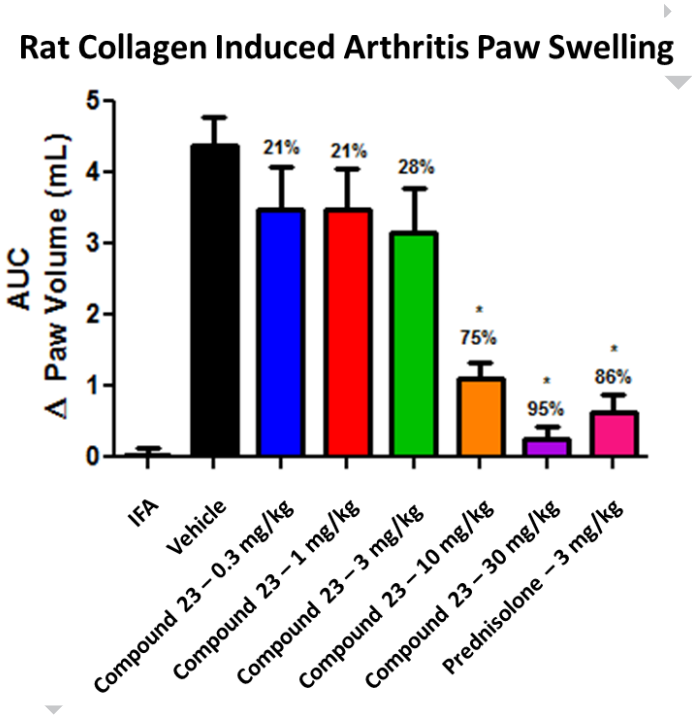

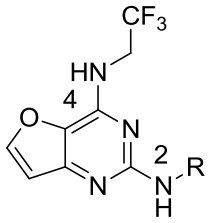

Compound	R	Syk IC_{50} (μM)[a]	Ramos B-Cell EC_{50} (μM)[b]	Rat Cl,mic unbound (L/hr/kg)	LLE
6	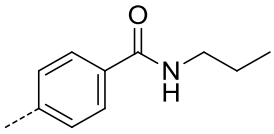	0.561	0.346	No Data	1.73
7	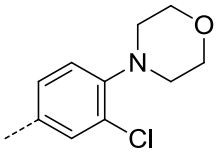	0.061	0.117	96.0	2.25
8	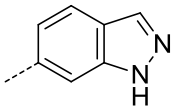	0.081	0.235	15.3	2.82
9	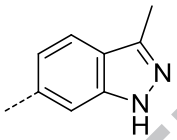	0.047	0.087	No Data	2.79
10	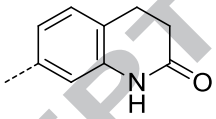	0.063	0.101	21.9	3.34
11	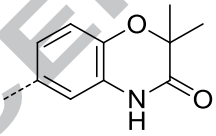	0.179	0.723	10.6	3.05
12	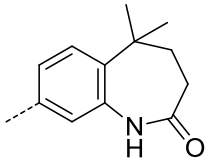	0.043	0.049	52.8	2.07
13	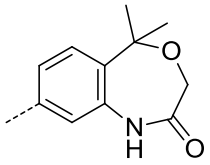	0.007	0.017	<4.9	5.10

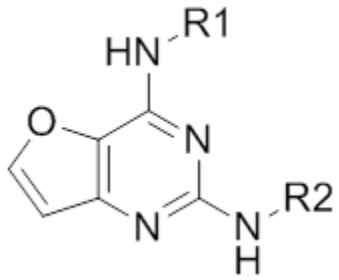

Compound	R1	R2	Syk IC_{50} (μM)[a]	Ramos B-Cell EC_{50} (μM)[b]	Rat Cl,mic unbound (L/hr/kg)	Human Cl,mic unbound (L/hr/kg)	Solubility Fed SSIF pH5 (μM)	LLE
13	$-CH_2CF_3$	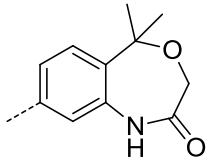	0.007	0.017	<4.9	10.2	4.96	5.10
14	$-CH_2CH_3$	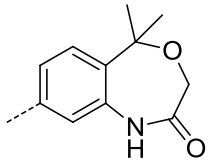	0.006	0.018	19.1	5.5	>67	5.43
15	$-CH_2CH_2CH_3$	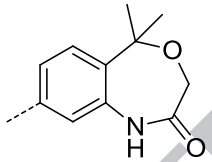	0.045	0.030	22.4	18.4	>200	4.03
16	$-CH_2CH_2(CH_3)_2$	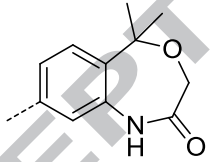	0.064	0.043	64.5	30.4		3.47

17	- $CH_2(CH_3)_2$	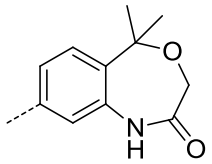	0.013	0.030				4.79
18	-c-Pr	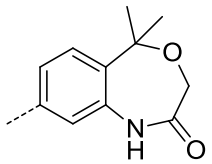	0.005	0.018	12.0	7.2	158	5.45
19	-c-Pr	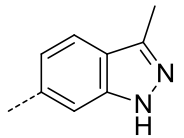	0.023	0.034			99	3.3
20	-c-Pr	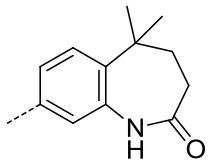	0.005	0.035	23.8	19.0		3.21
21	-c-Pr	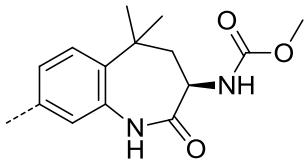	0.012	0.039	10.9	7.4	27	4.31
22	-c-Pr	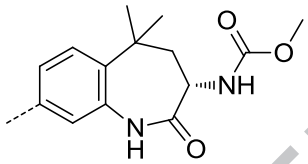	1.37		19.9	7.1		2.25
23	-CH_2CHF_2	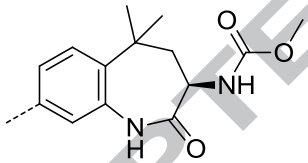	0.020	0.026	10.6	<2.3	>67	4.10